Pergamon

0734-743X(95)00048-8

Int. J. Impact Engng Vol. 18, No. 5, pp. 465–476, 1996

0734-743X/96 $15.00 + 0.00

PENETRATION OF GROUT AND CONCRETE TARGETS WITH OGIVE-NOSE STEEL PROJECTILES

M. J. FORRESTAL†, D. J. FREW‡, S. J. HANCHAK§, and N. S. BRAR§

† Sandia National Laboratories, Albuquerque, NM 87185-0312, U.S.A. ‡ Waterways Experiment Station, Vicksburg, MS 39180-6199, U.S.A. and § University of Dayton Research Institute, Dayton, OH 45469-0182, U.S.A.

(*Received* 13 *July* 1995; *in revised form* 9 *September* 1995)

Summary— We conducted depth of penetration experiments into grout and concrete targets with ogive-nose steel projectiles. Powder guns launched 0.064 kg, 12.9 mm diameter projectiles into grout targets with unconfined compressive strengths of 13.5 MPa (2.0 ksi) and 21.6 MPa (3.1 ksi). For the concrete targets, powder guns launched projectiles with length-to-diameter ratios of 10; a 0.48 kg, 20.3 mm diameter rod, and a 1.60 kg, 30.5 mm diameter rod. Concrete targets had unconfined compressive strength of 62.8 MPa (9.1 ksi) for the 0.48 kg rods and unconfined compressive strength of 51.0 MPa (7.4 ksi) for the 1.60 kg rods. For these experiments, penetration depth increased as striking velocity increased until nose erosion became excessive. Thus, we determined experimentally the striking velocities corresponding to maximum penetration depths. Predictions from a previously published model are in good agreement with data until nose erosion becomes excessive. Copyright © 1996 Elsevier Science Ltd.

Keywords: penetration, concrete targets, ogive-nose steel, nose erosion, striking velocities, compressive strength.

INTRODUCTION

Studies concerned with the penetration of concrete targets have focused on depth of penetration experiments and model development for striking velocities to 800 m/s [1]. In this study, we present new data for grout and concrete targets for striking velocities between 400 and 1700 m/s. This work provides additional data for model [1] verification and determines the striking velocities corresponding to maximum penetration depth and projectile failure.

Our model [1] describes the targets with density ρ_t, unconfined compressive strength f'_c, and an empirical constant S that depends only on f'_c; the projectiles are described with mass m, shank diameter $2a$, and caliber-radius-head ψ. However, concrete targets have more scales than those required for the analysis of ductile metal targets [2]. Table 1 lists parameters for the targets and projectiles. In addition to those parameters required for model [1] input, we list nominal aggregate diameter d, Moh's hardness scale [3] for the quartz-based aggregate, and Rockwell hardness R_c for the 4340 steel projectiles.

In the next sections, we describe our experiments, discuss our results, and compare data with model predictions.

PENETRATION EXPERIMENTS WITH GROUT TARGETS

We conducted three sets of experiments with the 0.064 kg, 12.9 mm diameter steel projectiles dimensioned in Fig. 1. Table 1 gives the material and geometric parameters for the grout targets and projectiles. Projectiles with 3.0 and 4.25 caliber-radius-head nose shapes were machined from 4340 steel rods and heat treated to a hardness of R_c 38–40. For striking velocities V_s between 350 and 1200 m/s, projectile shank diameters were centerless ground to fit snugly into the bore of a 12.9 mm powder gun, so projectiles were launched without sabots or obturators. To obtain striking velocities between 1200 and 1700 m/s, we used a 32 mm powder gun, so the projectiles were fitted with sabots and obturators that were stripped from the projectile before target impact. Two laser diode systems measured striking velocities, and orthogonal X-rays measured pitch and yaw angles.

12.9 mm diameter projectiles and 13.5 MPa (2.0 ksi) grout targets

Grout targets were cast in 0.30 m diameter fiber-reinforced cardboard tubes commercially available for pouring structural columns, and three 102 mm diameter, 203 mm long cylinders

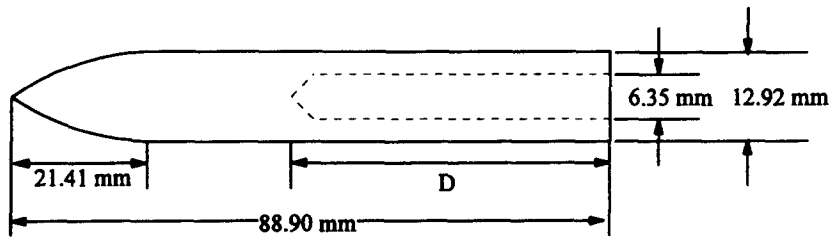

(a)

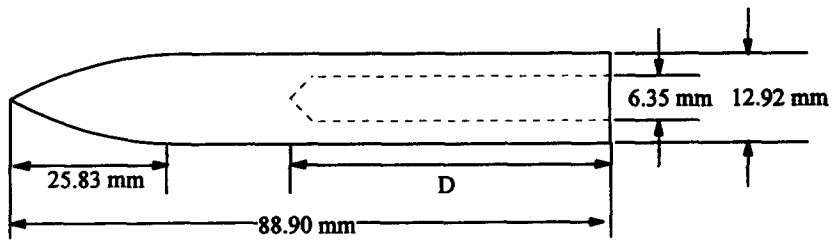

(b)

Fig. 1. Projectile geometries for the grout targets. Caliber-radius-head $\psi = 3.0$ for (a) and $\psi = 4.25$ for (b). D = approximately 50.8 mm, adjusted to obtain 0.064 kg.

Table 1. Penetration parameters

	Targets			
f'_c(MPa)	13.5	21.6	62.8	51.0
ρ_t(kg/m^3)	2000	2000	2300	2300
d(mm)	4.8	4.8	9.5	9.5
Moh's	7	7	7	7
S	20.2	15.2	8.6	10.5
	Projectiles			
m(kg)	0.064	0.064	0.48	1.60
$2a$(mm)	12.9	12.9	20.3	30.5
ψ	3.0, 4.25	3.0, 4.25	3.0	3.0
R_c	39	39	45	45

were cast for unconfined compressive strength tests. In addition, four 102 mm diameter, 203 mm long cylinders and two 50.8 mm diameter, 109 mm long cylinders were cored from a target for unconfined compressive strength tests. We tested nine grout cylinders and measured $f'_c = 11.7$–15.0 MPa with an average of $f'_c = 13.5$ MPa. Penetration and unconfined compressive strength experiments were conducted from 90 to 120 days after the grout was cast.

Table 2 summarizes the experimental results for the 0.30 m diameter targets with nominal unconfined compressive strength $f'_c = 13.5$ MPa (2.0 ksi). These data show an increase in penetration depth and projectile mass loss for increasing striking velocities to about 1100 m/s. Some of these data were reported previously in [1].

12.9 mm diameter projectiles and 21.6 MPa (3.1 ksi) grout targets

Grout targets were cast in 0.41 m diameter fiber-reinforced cardboard tubes, and three 102 mm diameter, 203 mm long cylinders were cast for unconfined compressive strength

Table 2. Penetration data for the 0.30 m diameter grout targets with nominal f'_c = 13.5 MPa (2.0 ksi). For pitch and yaw D = down, U = up, R = right, L = left

Shot number	Nose shape (CRH)	Target length (m)	Striking velocity (m/s)	Pitch yaw (deg)	Penetration depth (m)	Projectile mass loss (%)
6-2374	3.0	0.31	371	0.2D, 0.0	0.13	1.1
6-2363	3.0	0.60	590	0.4D, 0.7R	0.31	2.7
6-2367	3.0	0.63	670		0.36	3.4
6-2364	3.0	0.62	722	0, 0.5R	0.41	3.9
6.-2370	3.0	1.04	945	0.5D, 0.3R	0.64	4.6
6-2368	3.0	1.03	1126	1.0D, 0.5R	0.85	5.3
6-2373	4.25	0.31	345	0.4D, 0.2R	0.11	1.1
6-2362	4.25	0.62	585	0, 1.8L	0.31	3.3
6-2365	4.25	0.62	722		0.44	4.4
6-2371	4.25	1.03	900	0.7U, 0.3R	0.66	5.7
6-2369	4.25	1.02	1063	0.7D, 0.2R	0.86	6.3

tests. We tested the three cylinders at 170 days and measured f'_c = 21.5, 21.6, and 21.7 MPa with an average of f'_c = 21.6 MPa (3.1 ksi). Penetration tests were conducted between 150 and 210 days after the grout was cast.

Table 3 summarizes the experimental results for the 0.41 m diameter targets with nominal unconfined compressive strength f'_c = 21.6 MPa (3.1 ksi). These data show an increase in penetration depth and projectile mass loss for increasing striking velocities to about 1200 m/s. Figures 2 and 3 show photographs of the 3.0 and 4.25 caliber-radius-head projectiles that were recovered from the 0.41 m diameter targets and show the increase in nose erosion with increasing striking velocity.

12.9 mm diameter projectiles and 19.5 MPa (2.8 ksi) grout targets

Grout targets were cast in 0.48 m diameter plastic tubes, and six 102 mm diameter, 203 mm long cylinders were cast for unconfined compressive strength tests. We tested the six cylinders at 110 days and measured f'_c = 18.5–20.7 MPa with an average of f'_c = 19.5 MPa. Penetration tests were conducted from 110 to 130 days after the pour.

The first two sets of experiments into grout targets reported in Tables 2 and 3 were conducted to striking velocities of 1200 m/s, whereas this third set of experiments was conducted with striking velocities between 1300 and 1700 m/s. Table 4 summarizes the experimental results for the 0.48 m diameter targets with nominal unconfined compressive strength f'_c = 19.5 MPa. For the experiments conducted to striking velocities of 1200 m/s summarized in Tables 2 and 3, penetration depth increased as striking velocity increased and

Table 3. Penetration data for the 0.41 m diameter grout targets with nominal f'_c = 21.6 MPa (3.1 ksi). For pitch and yaw D = down, U = up, R = right, L = left

Shot number	Nose shape (CRH)	Target length (m)	Striking velocity (m/s)	Pitch yaw (deg)	Penetration depth (m)	Projectile mass loss (%)
6-2460	3.0	0.76	492	1.2D, 0.7R	0.17	1.8
6-2467	3.0	1.02	618	0.5U, 1.5D	0.25	2.0
6-2461	3.0	1.02	788	1.5D, 0.5R	0.45	5.3
6-2469	3.0	1.27	910	0.2U, 1.0R	0.55	6.8
6-2464	3.0	1.27	1029	0, 0.7R	0.75	6.9
6-2466	3.0	1.27	1142	0.5U, 0.7R	0.85	7.0
6-2459	4.25	0.76	473		0.17	1.9
6-2468	4.25	1.27	660	0.7U, —	0.27	4.0
6-2462	4.25	1.02	775	1.5U, 0.5L	0.41	5.0
6-2470	4.25	1.27	921		0.57	7.3
6-2463	4.25	1.27	1050	1.0U, 0.5R	0.76	7.9
6-2465	4.25	1.27	1190	1.7U, 0	0.88	7.5

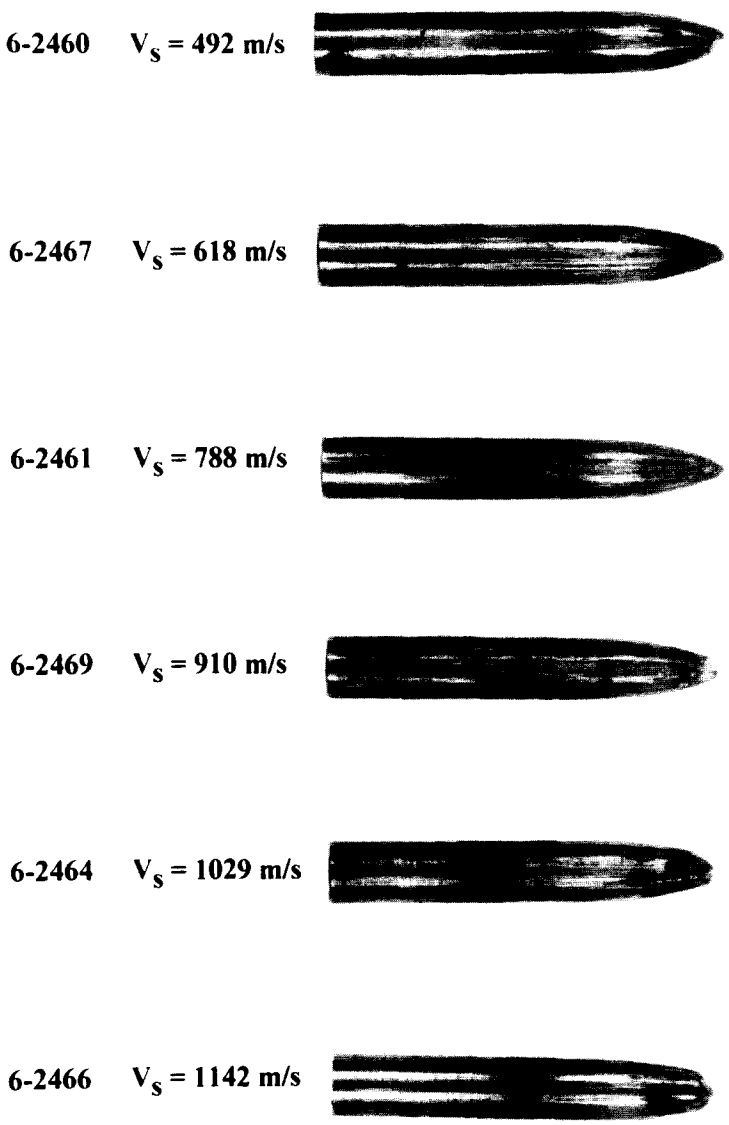

Fig. 2. Post-test photographs of the 3.0 caliber-radius-head projectiles recovered from the 0.41 m diameter, $f'_c = 21.6$ MPa grout targets.

the projectile trajectories had only minor deviations from the target centerlines. However, when striking velocities were increased to 1300–1700 m/s, the projectile trajectories deviated severely from the target centerlines. Asymmetric nose erosion and indentation of the projectile nose from the aggregate caused the projectiles to exit the side of the target, bend severely, or break.

PENETRATION EXPERIMENTS WITH CONCRETE TARGETS

We conducted two sets of penetration experiments with the 3.0 caliber-radius-head, 4340 steel rods dimensioned in Fig. 4. Table 1 gives the material and geometric parameters for the concrete targets and projectiles.

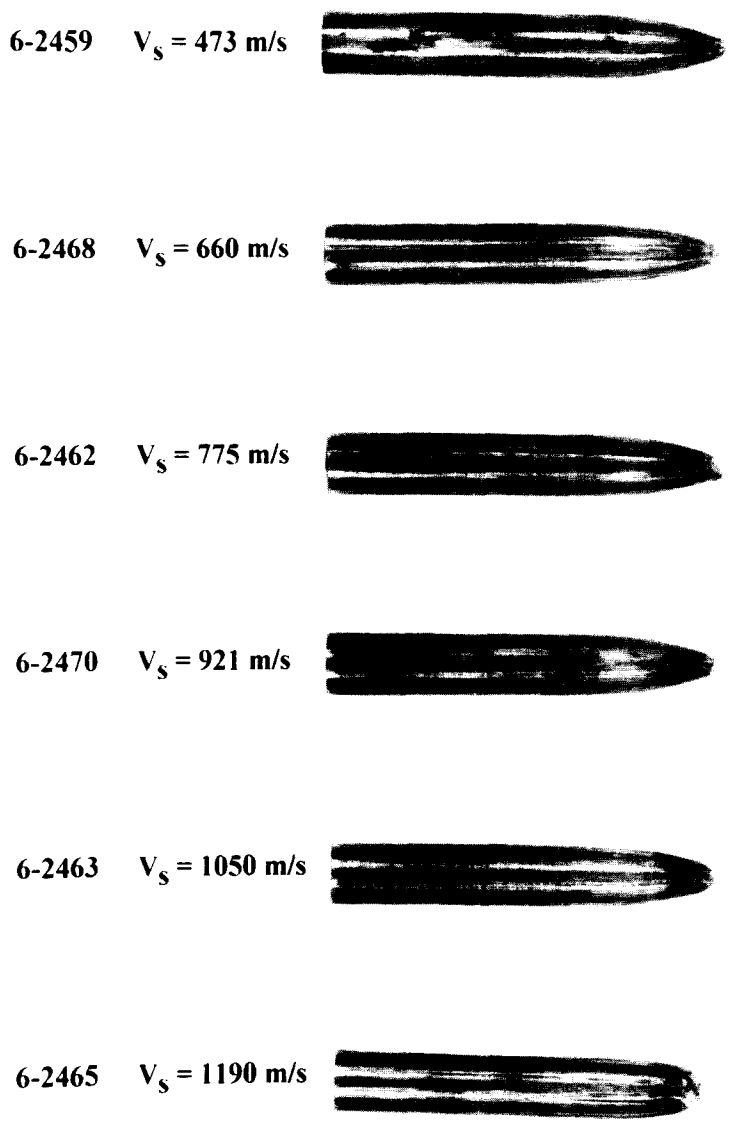

Fig. 3. Post-test photographs of the 4.25 caliber-radius-head projectiles recovered from the 0.41 m diameter, f'_c = 21.6 MPa grout targets.

20.3 mm diameter projectiles and 62.8 MPa (9.1 ksi) concrete targets

A 32 mm diameter smooth-bore powder gun launched the 0.48 kg projectiles dimensioned in Fig. 4(a) to striking velocities V_s between 450 and 1224 m/s. The projectiles were fitted with sabots and obturators that were stripped from the projectile during target impact. Four laser diode systems measured striking velocities, and orthogonal flash X-rays measured pitch and yaw angles.

Concrete targets were cast in approximately 0.51 m diameter PVC tubes and corrugated steel culverts. Four 51 mm diameter, 102 mm long cylinders were cored from a sample disk of a concrete target for unconfined compressive strength tests. We tested the concrete cylinders and measured f'_c = 56.0–70.2 MPa with an average of f'_c = 62.8 MPa. Penetration and unconfined compressive strength tests were conducted between 120 and 150 days after the concrete was cast.

Table 4. Penetration data for the 0.48 m diameter grout targets with nominal f'_c = 19.5 MPa (2.8 ksi). For pitch and yaw D = down, U = up, R = right, L = left

Shot number	Nose shape (CRH)	Target length (m)	Striking velocity (m/s)	Pitch yaw (deg)	Comments
1-0331	3.0	1.82	1356	1.0D, 1.1L	Trajectory turned from the centerline at 0.4 m and came to rest near the edge of the target with final depth 1.06 m.
1-0329	3.0	1.82	1408	0.4D, 0.0	Projectile bent to a 120° included angle with final penetration depth 0.58 m.
1-0330	3.0	1.82	1682	2.6U, 1.0L	Projectile fractured at the bottom of the drilled hole shown in Fig. 1.
1-0333	4.25	1.82	1311	1.8D, 2.2L	Projectile exited the side of the target at a depth of 0.78 m.
1-0334	4.25	1.82	1359	0.5D, 0.0	Projectile exited the side of the target at a depth of 1.0 m.
1-0332	4.25	1.82	1430	0.8D, 0.0	Projectile exited the side of the target at a depth of 0.84 m.

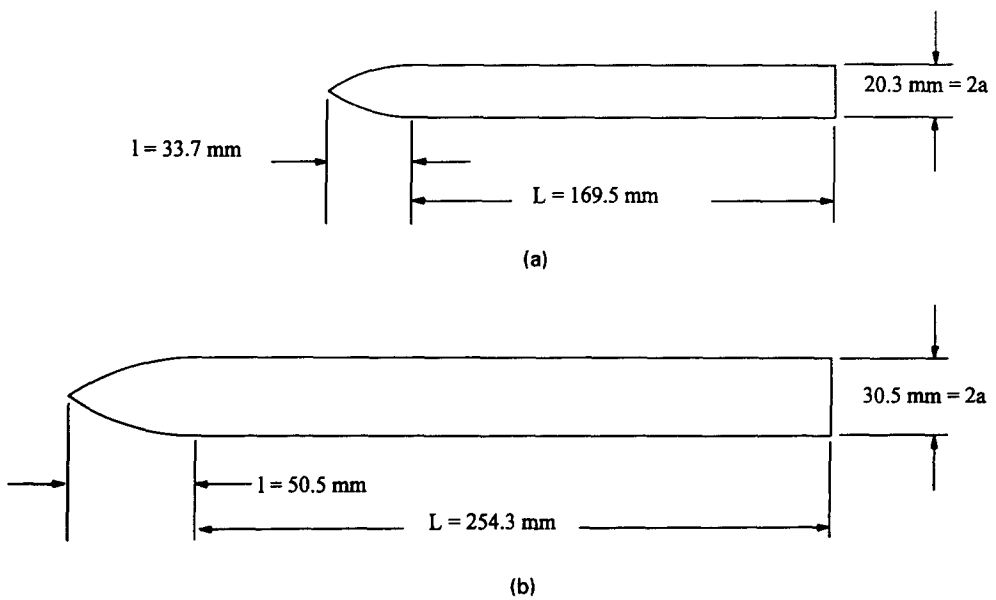

Fig. 4. Rod projectile geometries for the concrete targets. Caliber-radius-head $\psi = 3.0$ for both projectiles.

Table 5 summarizes the experimental results for the 20.3 mm diameter rods. The last column in Table 5 shows an increase in projectile mass loss for striking velocities to 987 m/s. Figure 5 shows post-test photographs of the ogive-nose rods that were recovered from the targets and also shows an increase in nose erosion with increasing striking velocity. For a striking velocity of 1224 m/s, the rod fractured in the target at a depth of 0.5 m.

30.5 mm diameter projectiles and 51.0 MPa (7.4 ksi) concrete targets

An 83 mm diameter smooth-bore powder gun launched the 1.60 kg projectiles dimensioned in Fig. 4(b) to striking velocities V_s between 405 and 1358 m/s. The projectiles were fitted with sabots and obturators that were aerodynamically stripped from the projectile

Table 5. Penetration data for the 0.51 m diameter concrete targets with nominal f'_c = 62.8MPa (9.1 ksi). For pitch and yaw D = down, U = up, R = right, L = left

Shot number	Projectile mass (kg)	Target length (m)	Striking velocity (m/s)	Pitch yaw (deg)	Penetration depth (m)	Projectile mass loss (%)
1-0335	0.478	0.91	450	0.0, 0.6R	0.30	1.5
1-0336	0.478	0.91	612	0.0, 0.4L	0.48	2.7
1-0337	0.478	1.22	821	0.0, 0.0	0.76	4.5
1-0341	0.478	1.52	926	0.5U, 0.1L	0.95	5.5
1-0346	0.478	1.52	987	0.2D, 0.0	0.92	6.6
1-0338	0.478	1.52	1024	0.2U, 0.0	0.94	6.2
1-0339	0.478	1.83	1224		Projectile fractured	

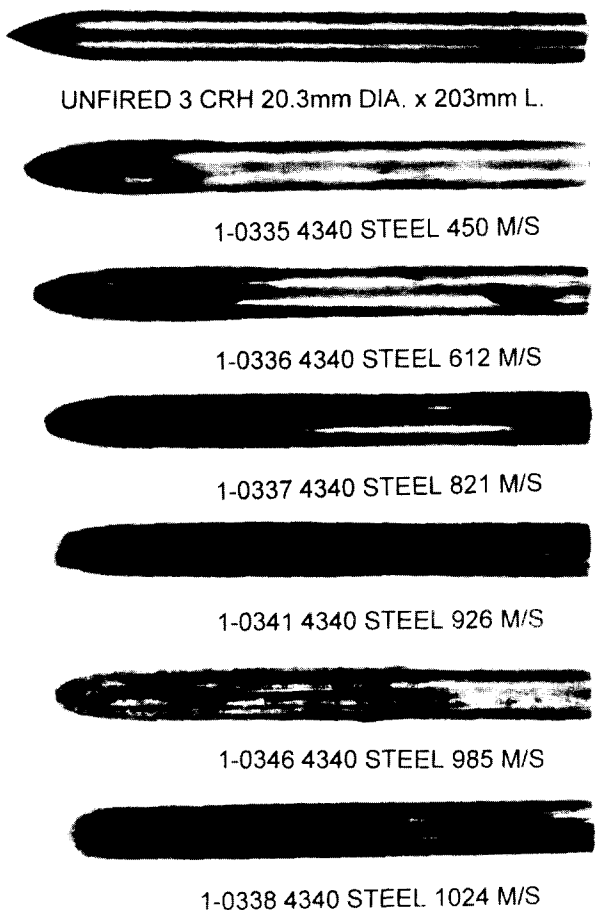

Fig. 5. Post-test photographs of the 20.3 mm diameter rods recovered from the f'_c = 62.8 MPa concrete targets.

before target impact. A Hall Intervalometer System measured striking velocities, and orthogonal flash X-rays measured pitch and yaw angles.

Concrete targets were cast in approximately 0.91 m diameter corrugated steel culverts. Four 51 mm diameter, 102 mm long cylinders were cored from a sample disk of a concrete target for unconfined compressive strength tests. We tested the concrete cylinders and measured f'_c = 48.3–55.2 MPa with an average of f'_c = 51.0 MPa. Penetration and unconfined compressive strength tests were conducted between 180 and 210 days after the concrete was cast.

Table 6 summarizes the experimental results for the 30.5 mm diameter rods. The last column in Table 6 shows an increase in projectile mass loss for striking velocities to 1069 m/s. Figure 6 shows post-test photographs of the ogive-nose rods that were recovered from the targets. For a striking velocity of 1358 m/s, the rod exited the side of the target at a depth of 1.8 m.

OGIVE-NOSE ROD PENETRATION MODEL

Forrestal *et al.* [1] present an analytical penetration equation for rigid ogive-nose projectiles and concrete targets. This penetration equation contains a single, dimensionless-empirical constant S for fixed values of unconfined compressive strength f'_c of the concrete target. For an ogive-nose, solid-rod projectile, the penetration equations in [1] can be put in a form that displays clearly the problem parameters.

As shown in [4], an ogive is the arc of the circle tangent to the shank. It is common to define the ogive in terms of caliber-radius-head

$$\mathrm{CRH} = \frac{s}{2a} = \psi \tag{1a}$$

where s is the circle radius and $2a$ is the shank diameter. In addition [4], the nose length and projectile mass are given by

$$l = a(4\psi - 1)^{1/2} \tag{1b}$$

$$m = \pi a^2 \rho_p (L + ka) \tag{1c}$$

$$k = \left(4\psi^2 - \frac{4\psi}{3} + \frac{1}{3}\right)(4\psi - 1)^{1/2} - 4\psi^2(2\psi - 1)\sin^{-1}\left[\frac{(4\psi - 1)^{1/2}}{2\psi}\right] \tag{1d}$$

where L is shank length, l is nose length, and ρ_p is projectile density.

Substitution of (1a–1c) into the penetration equations presented in [1] gives

$$P = \frac{(L + ka)}{2N}\left(\frac{\rho_p}{\rho_t}\right)\ln\left[1 + \frac{N\rho_t V_1^2}{Sf'_c}\right] + 4a, \quad P > 4a \tag{2a}$$

$$N = \frac{8\psi - 1}{24\psi^2} \tag{2b}$$

$$V_1^2 = \frac{V_s^2 - \left(\frac{4a}{L + ka}\right)\left(\frac{Sf'_c}{\rho_p}\right)}{1 + N\left(\frac{4a}{L + ka}\right)\left(\frac{\rho_t}{\rho_p}\right)}. \tag{2c}$$

Table 6. Penetration data for the 0.91 m diameter concrete targets with nominal f'_c = 51.0 MPa (7.4 ksi). For pitch and yaw D = down, U = up, R = right, L = left

Shot number	Projectile mass (kg)	Target length (m)	Striking velocity (m/s)	Pitch yaw (deg)	Penetration depth (m)	Projectile mass loss (%)
LROD-2	1.608	1.83	405	2.3U, 0.3L	0.37	1.2
LROD--3	1.600	1.83	446		0.42	1.5
LROD-6	1.600	2.13	545	1.0U, 1.0L	0.56	2.0
LROD-4	1.603	2.13	651	1.2U, 0.7L	0.78	3 1
LROD-8	1.604	2.13	804	1.0U, 0.1L	1.05	4.7
LROD-5	1.600	2.13	821	0.4U, 0.4L	1.23	4.4
LROD-9	1.603	2.44	900	1.0U, 0.3L	1.41	5.4
LROD-10	1.599	2.44	1009	0.4U, 0.4L	1.75	6.4
LROD-11	1.609	2.74	1069	0.6U, 0.7L	1.96	7.0
LROD-12	1.603	2.74	1201	0.3D, 0.4L	2.03	6.8
LROD-13	1.603	2.74	1358	0.1U, 0.7L		Projectile exited side of target

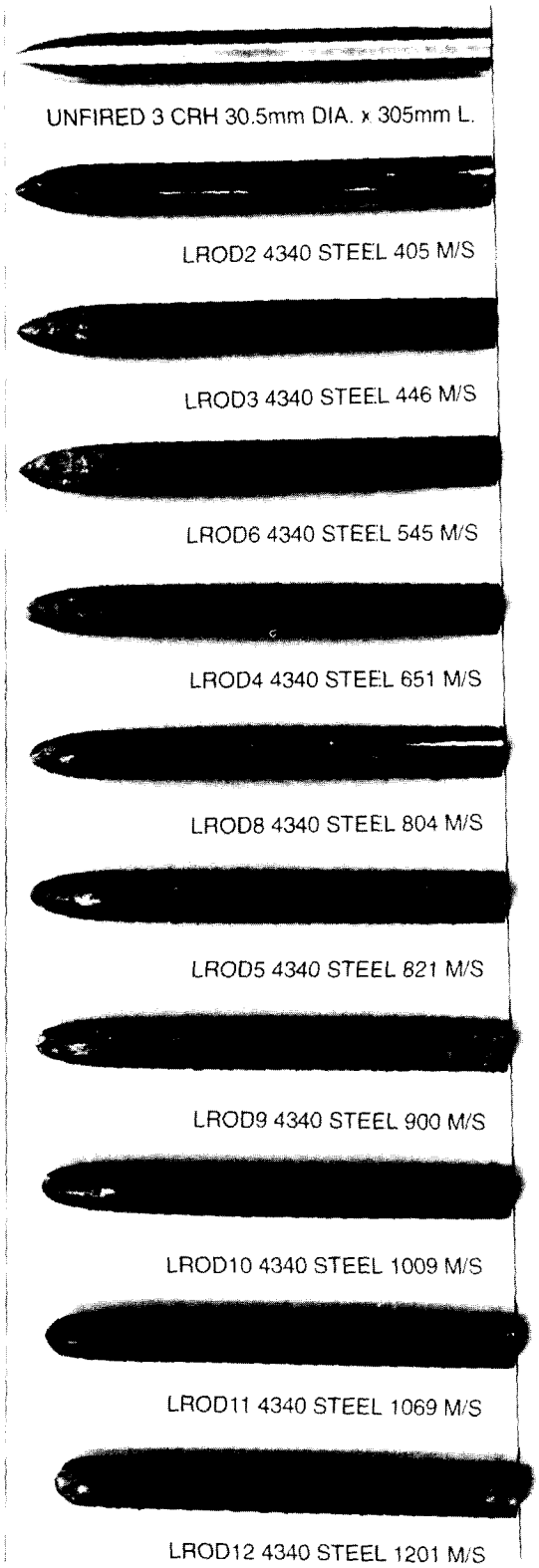

Fig. 6. Post-test photographs of the 30.5 mm diameter rods recovered from the $f'_c = 51.0$ MPa concrete targets.

In Eqns (2a–2c), P is penetration depth, V_s is striking velocity, V_1 is projectile velocity at penetration depth $4a$, f'_c is unconfined compressive strength, ρ_t is target density, and S is a dimensionless empirical constant that depends on f'_c [1]. The relation between S and f'_c is given later.

RESULTS

As explained in [1], the dimensionless empirical constant S in the depth of penetration equations given in [1] and by Eqns (2a–2c) for the special cases of solid-rod projectiles depends only on the unconfined compressive strength of the target f'_c. The value of S is determined from data sets of penetration depth P and striking velocity V_s for a fixed value of f'_c. Figures 7 and 8 show data and model predictions [1] for the projectiles shown in Fig. 1 that were launched into the 13.5 MPa and 21.6 MPa grout targets. As previously mentioned, for striking velocities greater than 1200 m/s, the projectile exited the side of the target, bent severely, or broke. Figure 9 shows data and model predictions from Eqns (2a–2c) for the

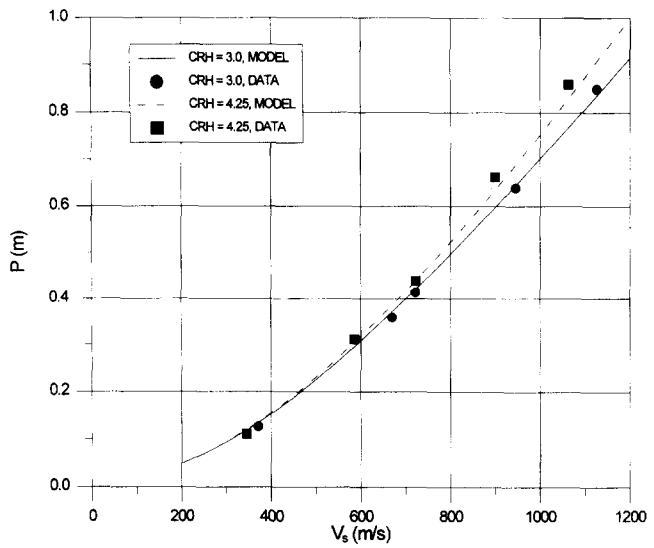

Fig. 7. Data and model prediction [1] for grout targets with $f'_c = 13.5$ MPa and $S = 20.2$.

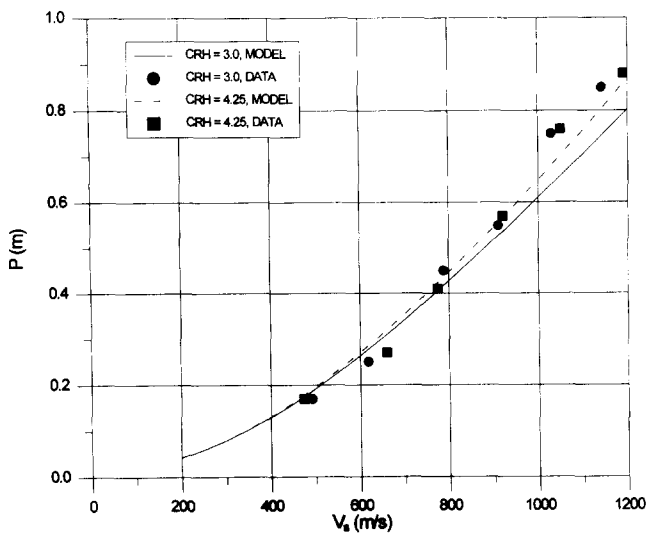

Fig. 8. Data and model prediction [1] for grout targets with $f'_c = 21.6$ MPa and $S = 15.2$.

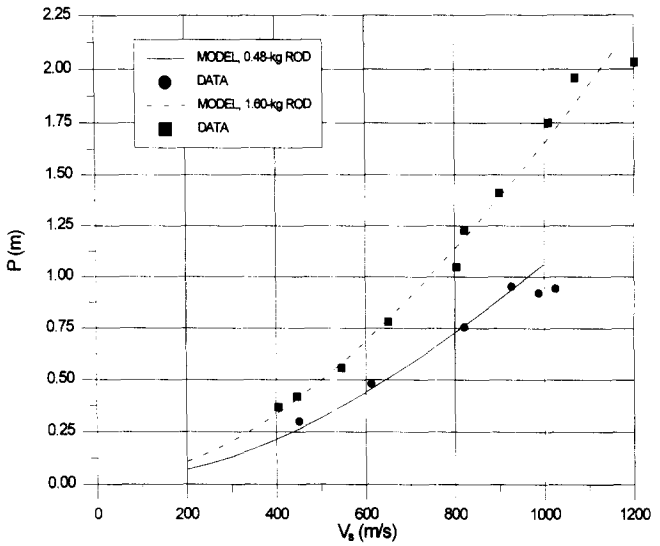

Fig. 9. Data and model predictions [1] for the concrete targets. For $f'_c = 62.8$ MPa, $S = 8.6$. For $f'_c = 51.0$, $S = 10.5$.

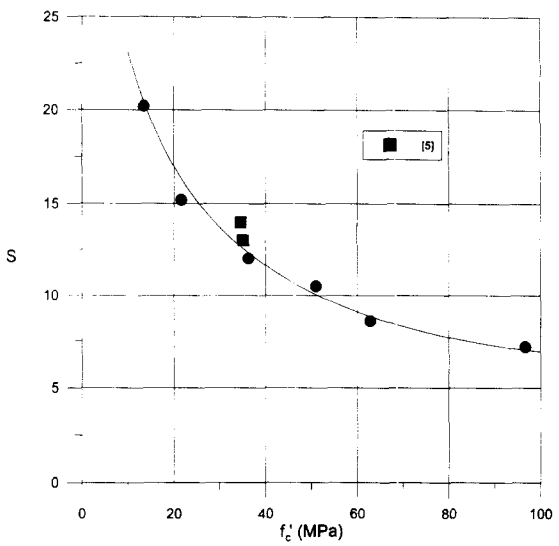

Fig. 10. Dimensionless empirical constant vs unconfined compressive strength.

solid-rod projectiles shown in Fig. 4 that were launched into the 51.0 MPa and 62.8 MPa concrete targets. Data in Fig. 9 show that depth of penetration increased as striking velocity increased and then reached a plateau. Tables 5 and 6 show that for a further increase in striking velocity, the rods fractured or exited the side of the target.

With the new data presented in this paper and some of the data presented in [1], we revised the empirical curve that relates S to f'_c. Figure 10 shows the relationship between S and f'_c, which was curve-fit to available data for grout and concrete targets that had no reinforcement. Figure 10 also shows data from Canfield and Clator [5] for reinforced concrete targets.

CONCLUSIONS

We presented depth-of-penetration vs striking-velocity data for projectiles launched into grout and concrete targets. Striking velocity was increased until nose erosion became excessive and the projectiles exited the side of the target, bent severely, or broke. Thus, we determined experimentally the striking velocities corresponding to maximum depth of

penetration. Predictions from a previously published model [1] are in good agreement with data until nose erosion becomes excessive.

Acknowledgements– This work was sponsored by the Joint DoD/DoE Munitions Technology Program and the U.S. Army Corps of Engineers Hardened Structures Research Program. The authors gratefully acknowledge permisson from the Office, Chief of Engineers to publish this paper.

REFERENCES

1. M. J. Forrestal, B. S. Altman, J. D. Cargile and S. J. Hanchak, An empirical equation for penetration depth of ogive-nose projectiles into concrete targets. *Int. J. Impact Engng* **15**, 395–405 (1994).
2. M. J. Forrestal, D. Y. Tzou, E. Askari and D. B. Longcope, Penetration into ductile metal targets with rigid spherical-nose rods. *Int. J. Impact Engng* **16**, 699–710 (1995).
3. R. C. Weast, *CRC Handbook of Chemistry and Physics*. CRC Press, F-24 (1980).
4. M. J. Forrestal, V. K. Luk, Z. Rosenberg and N. S. Brar, Penetration of 7075-T651 aluminum targets with ogival-nose rods. *Int. J. Solids Struct.* **29**, 1729–1736 (1992).
5. J. A. Canfield and I. G. Clator, Development of a scaling law and techniques to investigate penetration in concrete. NWL Report No. 2057, U.S. Naval Weapons Laboratory, Dahlgren, VA (1966).